06

Analysis of the effect of yield stress on stress corrosion cracking of martensitic and ferritic steels in acidic environments

© A.I. Petrov, M.V. Razuvaeva

Ioffe Institute,
St. Petersburg, Russia
e-mail: An.Petrov@mail.ioffe.ru, M.Razuvaeva@mail.ioffe.ru

Received June 13, 2022
Revised July 3, 2022
Accepted July 4, 2022

To evaluate the effect of yield stress on hydrogen embrittlement (HE) of martensitic and ferritic steels, the effect of hydrogen (H) capture by structural inhomogeneities (hydrogen traps) and the effect of plastic deformation and stress on the mechanism of stress corrosion cracking (SCC) are considered. In the presence of hydrogen, the brittle fracture of high-strength martensitic steels consists of flat areas of intergranular fracture at the initial austenitic grain boundaries and quasi-brittle cracks at the boundaries of martensite blocks. In low-strength steels, brittle fracture manifests itself in the form of transgranular fracture of ferrite grains. The decrease in the characteristics of martensitic steels with an increase in the yield strength occurs due to an increase in the hydrogen concentration at the stage of anodic dissolution (AD) due to the growth of the carbide/matrix interface. The reason for the growth hydrogen concentration in ferritic steels is a large mechanical overstress, an increase in the number of active dissolution centers, the formation of an electrochemical pearlite-ferrite pair, and an increase in surface roughness with increasing deformation. It is concluded that the bell-shaped dependences of the critical stress of the transition from AD to SCC and other characteristics of mechanical tests on magnitude of the yield stress are due to different mechanisms of hydrogen accumulation in martensitic and ferritic steels.

Keywords: hydrogen embrittlement, high-angle boundaries, interfaces, traps, hydrogen binding energy, structural inhomogeneities, fracture.

DOI: 10.21883/TP.2022.10.54364.154-22

Introduction

In previous work [1] it was shown that in the NACE solution in the region of active corrosion at constant stress of low-alloyed martensitic and ferritic pipe steels, the value of the overstress coefficient (K_T) in the range of yield stress σ_{02} from 550 to 1100 MPa is constant at 1.4. For σ_{02} less than 550 MPa, the value K_T jumps up to a value equal to 4.1. For these steels, it was also revealed that the dependence of the critical stress (σ_{CR}) of the transition from active corrosion to corrosion caused by hydrogen embrittlement (HE) under stress (SCC) is bell-shaped with a maximum at σ_{02} about 550 MPa (Fig. 1). The present work is a continuation of the previously published one [1]. The paper analyzes data on the strength (σ_{02}) effect on the susceptibility of martensitic and ferritic steels to HE. The connection of hydrogen with microscopic heterogeneities, which act as traps for hydrogen, and their influence on the fracture process, the influence of stress and plastic deformation on electrochemical reactions, the morphology of the fracture surface, and other structural features that affect the susceptibility of steel to HE are discussed.

The purpose of this paper is to establish the mechanisms of corrosion cracking responsible for the bell-shaped dependence of SCC on the value σ_{02} of high-strength medium-alloyed Ni–Cr–Mo-martensitic steels hardened by nanosized particles and low-alloyed ferritic pipe steels in acidic environment containing H_2S.

HE means that hydrogen, arising in the process of cathodic reactions, or penetrating from the environment, migrates in the form of atomic hydrogen to internal centers of high stresses, leading to fracture. Three main fracture mechanisms were proposed: hydrogen-enhanced decohesion (HEDE) [2,3], hydrogen-enhanced localized

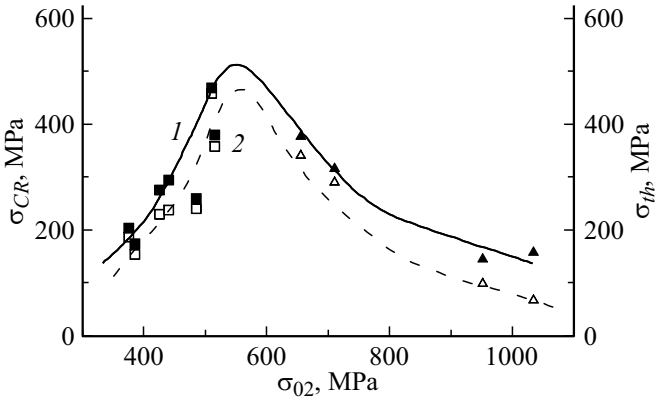

Figure 1. Critical stress (σ_{CR}) of the transition from the anodic dissolution (AD) to the SCC stage and the threshold stress during the test 720 h (σ_{th}) in NACE solution for ferritic (□, ■) and martensitic (△, ▲) steels vs. the yield stress (σ_{02}): curve *1*(▲, ■) — σ_{CR}, curve *2*(△, □) — σ_{th}.

plasticity (HELP) [4,5], hydrogen-enhanced vacancy stabilization mechanism (VM) [6]. According to the HEDE mechanism, the accumulation of hydrogen at grain boundaries or interfaces of particles of the second phase leads to weakening of cohesive bonds and subsequent fracture. In the HELP mechanism, it is shown that the injection of hydrogen increases the mobility of dislocations and causes localization of plastic deformation. In the case of VM, it was shown that deformation in the presence of hydrogen leads to the accumulation of excess vacancies, the formation of microvoids, and subsequent fracture due to their coalescence.

Damage to steel under conditions of hydrogen pickup is determined by the amount of trapped hydrogen by various traps. Such traps are microstructural heterogeneities: substitutional atoms, vacancies, dislocations, various inclusions, micropores, elastic stress fields [7,8]. The trapping sites are characterized mainly by the binding energy W_B. Traps with binding energy $W_B > 60$ kJ/mol are strong and irreversible, traps with binding energy $W_B < 30$ kJ/mol are weak and reversible [9]. It was established that, first of all, hydrogen is trapped by strong traps; weak traps are not filled with hydrogen until strong traps are filled. Weak traps are dislocations ($W_B = 20-30$ kJ/mol), coherent inclusion M_2C and carbides ($W_B = 11.5$ kJ/mol), cementite interfaces ($W_B = 11-18$ kJ/mol), ferrite grain boundaries ($W_B = 32$ kJ/mol), lattice traps with weak filling — atoms Cr, Mo, V, Ti ($W_B = 26-27$ kJ/mol) dissolved in the matrix, low-angle grain boundaries of plates in martensitic steels, consisting of edge and screw dislocations with binding energy ($W_B = 15-35$ kJ/mol) [10]. Strong traps are high-angle initial austenitic grain boundaries with energy $W_B = 40-60$ kJ/mol, as well as interfaces between particles at the grain boundaries and the matrix [11]: MnS (72 kJ/mol), iron oxides 51−70 kJ/mol. Also strong traps are vacancies $W_B = 49-51$ kJ/mol [12], dislocation cores 51.6 kJ/mol [10], vacancy clusters 68 kJ/mol [10,12].

Hydrogen trapped in traps is in local equilibrium with the lattice. If W_B is small, then the trapped hydrogen can act at room temperature as an additional source of hydrogen. The source begins to operate when the hydrogen concentration in the matrix is below the equilibrium value. Such hydrogen is classified as diffusive, which can migrate, for example, to the area of stress concentration near the crack tip [13]. For this reason, the increased number of traps with low binding energy rises the concentration of hydrogen in the matrix. This hydrogen can be trapped by dislocations and moved by them to different places with high energy W_B. On the contrary, the presence in the steel of a large number of strong traps capable of trapping hydrogen, for example, finely dispersed carbides, improves the steel resistance to HE [11].

For martensitic steels, the total amount of hydrogen increases during tempering due to the formation of a large amount of carbides [14]. It was found that the ability of carbides to trap hydrogen depends on their size. Thus, it was established that TiC carbides larger than 70 nm are not capable of trapping hydrogen. For $Cr_{23}C_6$ carbides the critical value is 100 nm, for Mo_2C — 75 nm, and for carbides V_4C_3 and W_2C the particles larger than 20 nm cannot trap hydrogen [15]. In addition to the size, a strong factor determining the ability to trap hydrogen is the coherence of the carbide/matrix [8] interface. Thus, for incoherent TiC particles in steel 0.42C−0.30Ti, the value W_B is 85 kJ/mol, while for coherent TiC particles in this steel W_B is 35 kJ/mol [16].

Thus, irreversible traps function at low temperatures as hydrogen absorbers, which improves the corrosion properties of steels. Weak traps provide a reservoir of mobile hydrogen that diffuses into damage sites and contributes to the hydrogen embrittlement of steel.

Dislocations are the main type of traps with maximum occupancy and binding energy, which makes it possible to deliver hydrogen to damage sites. Moving dislocations trap hydrogen dissolved in the lattice only when the speed of their movement approximately coincides with the diffusion speed of hydrogen atoms in the lattice [7,17]. For this reason HE is observed only at strain rates $\dot{\varepsilon} \approx 10^{-5}-10^{-6}\,\mathrm{s}^{-1}$, and is not observed at strain rates $\dot{\varepsilon} \approx 10^{-3}\,\mathrm{s}^{-1}$. Note that if the density of traps at grain and carbide boundaries is constant and does not depend on strain, then the density of traps on dislocations N_T^D increases with strain in proportion to the increasing of the dislocation density ρ: $N_T^D = \sqrt{2}\rho/a$ (a — lattice parameter). It was also established that when a hydrogen atom is bound to dislocations cores, the dislocation mobility increases by an order of magnitude, and the dislocation line energy and the Peierls stress decrease. The presence of hydrogen prevents the cross slip of dislocations by increasing the distance between partial dislocations, which contributes to the formation of localized shear bands. Hydrogen-induced increasing of the number of dislocations in flat pilling up leads to the creation of high stresses in the head of the pilling up and thus to stress increasing when the pilling up collide with brittle inclusions at the grain boundary [18–20].

High-strength martensitic steels have a four-level hierarchy of microstructures, consisting of grain boundaries of the original austenite, a package, a block, and a plate boundary [21]. Among these boundaries, high-angle grain boundaries that can impede the movement of dislocations, leading to the accumulation of dislocations at the boundary, are initially austenitic grain boundaries and block boundaries. They are boundaries with a high angle of misorientation with a hydrogen binding energy of 47.4 kJ/mol [11]. The plate boundaries are low-angle boundaries consisting of edge and screw dislocations with the binding energy of $W_B = 26$ kJ/mol [11]dislocations. The substructure of the AISI 4340 martensitic alloy with strength $\sigma_{02} = 1100$ MPa consists of dislocations, cementite particles 90 nm in size located inside the plates, nanosized particles TiN, AlN, Al_2O_3 and MnS 6 nm in size dispersed in matrix [11]. Particles in the form of (Ti, Mo)C carbides are also observed.

The cementite/matrix interface is incoherent and its energy of binding with hydrogen is 10.9 kJ/mol [11]. With such a low value of W_B, these particles ≈ 90 nm in size cannot affect the susceptibility of steel to HE. Nanosized particles (Ti, Mo)C with the hydrogen binding energy $W_B = 30.5-52$ kJ/mol increase the resistance of steel to HE, since their presence leads to hydrogen decreasing in the lattice and in dislocations. TiN, AlN, Al_2O_3, MnS particles can also act as hydrogen traps, however, according to the authors of [11], they have an insignificant effect on hydrogen trap.

Thus, the main sites of hydrogen traps in high-strength martensitic steel are boundaries with a binding energy of 47.4 kJ/mol and dislocations. The dislocations density in AISI 4340 steel in the initial state is $7 \cdot 10^{13}\,\mathrm{m}^{-2}$, and after deformation $\varepsilon = 2\%$ it is $2.3 \cdot 10^{15}\,\mathrm{m}^{-2}$, and remains constant under deformation up to 28% [11]. Note that the plastic deformation of steel with a BCC lattice is determined by screw dislocations, and not by edge dislocations [22]. For this reason, in martensitic steels, hydrogen trap is considered in the cores of screw dislocations.

Let us review the data on the study of the morphology of the fracture surface of high-strength martensitic steel. In the absence of hydrogen at room temperature, fracture occurs due to the coalescence of micropores. In the presence of hydrogen, the fracture surface consists of a mixture of „flat“ regions that run along the original austenite grain boundaries and are classified as intergranular fracture, and quasi-cleavage surface that run along the slip planes {110} in martensite blocks. In this case, in contrast to flat fracture elements, the surface of the quasi-cleavage is not flat; it is curved and has small zigzag markings [11,23,24]. According to [7], the splitting energy is equal to twice the surface energy; the cohesive energy decreases linearly with increasing of hydrogen concentration. It was also shown [23] that the microstructure directly under both flat and quasi-cleavage surfaces contains intense localized slip bands. This allows us to conclude [11] that the hydrogen-induced fracture in loaded martensitic steels can be explained by the simultaneous action of the localized plasticity (HELP) and decohesion (HEDE) mechanisms. Intergranular fracture occurs when dislocation pilling up collide with the initial boundaries of austenite grains, and quasi-cleavage occurs when dislocation pilling up collide with high-angle block boundaries in martensite. As noted above, hydrogen increases the mobility of dislocations, which leads to severe plastic deformation in grains in the form of slip bands and a high density of dislocations. In turn, the increasing of the dislocation density rises the local concentration of hydrogen at the boundaries, which reduces the cohesive energy of the boundaries. Mechanical stresses, which are locally enhanced at high-angle boundaries, can also be attributed to the factors that enhance the fracture process.

The hydrogen printing method [23], in which AgBr is restored to Ag by hydrogen, was used to visualize the distribution of hydrogen atoms on the fracture surface. It is shown that hydrogen accumulation occurs near the high-angle boundaries of austenite grains and martensite blocks, which is consistent with the hydrogen transfer to these boundaries due to dislocation activity.

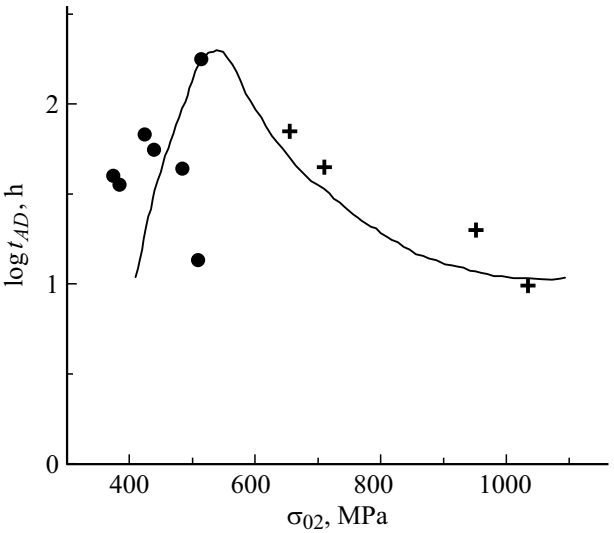

Figure 2. Duration of AD stage for low-alloyed ferritic (•) and high-strength martensitic steels (+) vs. value of the yield stress (σ_{02}).

Note that in the paper under consideration [11] the mechanism of fracture of martensitic steels proposed earlier by Novak [19] was substantially refined. Novak believed that the fracture occurs as a result of decohesion at the inclusion/matrix interface. It was found for the first time in paper [11] that fracture initiation sites are either high-angle initial austenite grain boundaries or martensite block boundaries. The indicated fracture mechanism of martensitic steels, based on the simultaneous action of the HELP and HEDE mechanisms, was also confirmed in other papers [22].

It was also found that stress corrosion cracking is significantly affected by the microstructure, the state in which hydrogen is in the steel (lattice hydrogen, hydrogen in traps, hydrogen in strong traps), the stressed state of the material, i.e., local stress σ_m value and value of equivalent plastic strain ε_{peq} [25].

The influence of the microstructure is quite well traced when studying the effect of annealing on the value of the yield stress σ_{02}, the amount of trapped hydrogen, the susceptibility of martensitic steels to HE, and the time of SCC beginning (Fig. 2). It was shown [26] that in a wide range of σ_{02} change from 655 to 1030 MPa, the amount of trapped hydrogen, as well as the susceptibility to HE under stress increase with strength increasing. Microstructural studies showed that under conditions of high strength, the size of carbides is smaller than under conditions of lower strength, but their concentration is much higher [26]. The latter means that smaller carbides in high strength martensitic steel will result in a larger carbide/matrix

interfacial area and correspondingly more trapped hydrogen. The high susceptibility to HE of martensitic steels in the high-strength state is also found in the critical stress σ_{CR} of the transition from the active corrosion stage to the HE stage dependence on the value σ_{02} (Fig. 1). A feature of this dependence is its bell-shaped nature with a maximum at $\sigma_{02} \cong 550$ MPa, i.e., at the transition point from martensitic steels to weaker pipe steels with a ferritic structure.

Let us discuss the features, caused by hydrogen, of the fracture of low-strength ferritic steels. The mechanical behavior of ferritic steels in the presence of hydrogen differs distinctly from that of martensitic steels. It was found that in iron and ferritic steels „brittle" fracture manifests itself in the form of transgranular quasi-fracture [20]. A complete intergranular rupture due to the cohesive strength decreasing of the grain boundary in the presence of hydrogen is found only under conditions of strong cathodic polarization at high current density. Under normal conditions of hydrogen pick up, grain boundaries, cementite particles, and carbides do not participate in the development of fracture. This is due to the low binding energy of hydrogen with the boundaries of ferrite grains (18−20 kJ/mol), cementite (19−23 kJ/mol) compared to the binding energy of hydrogen with dislocations (20−30 kJ/mol) [27]. Carbides in ferritic steel also have little effect on fracture. The binding energy of hydrogen at ferrite/Fe_3C interfaces is 11−18 kJ/mol only [27]. At the same time, the influence of various types of complex inclusions on the SCC of low-strength pipeline ferritic steels was found. So, in [28] for steel X70 ($\sigma_{02} \approx 440$ MPa) when the samples are tensioned in an acidic solution (pH = 4) with a low strain rate (SSRT) different behavior of inclusions enriched with Al_2O_3 and those enriched with SiO_2 was found. Cracks occur at inclusions enriched with aluminum. Note that such inclusions are hard, brittle, incoherent to the metal matrix and inclined to mechanical overstress [28]. At the same time, silicon-enriched inclusions are easily deformed and can effectively remove overstresses occurred under load, therefore, under SCC conditions cracks do not appear in such inclusions [29].

It was shown [30] that SCC in pipe steels (X80, $\sigma_{02} = 550$ MPa), in acid environment pH = 4 is controlled simultaneously by both anodic dissolution and HE. It was established that the initial sites of SCC initiation in pipe steels are MnS inclusions, which initiate pitting [28]. The stress concentration in the pits causes the local current increasing of anodic dissolution and, consequently, additional accumulation of hydrogen in the steel [30]. Besides, a noticeable acceleration of the dissolution process can occur due to the formation of an electrochemical pair ferrite-pearlite [31].

For ferritic steels, as well as for martensitic steels, the susceptibility to HE also changes with the increasing of steel strength. Thus, it was noted [26] that when testing round, precharging hydrogen speciments, the HE characteristics (deformation to fracture ε_f and the relative change in the cross-section area of the specimen at the moment of fracture RA) change significantly with the change of the value of the yield stress σ_{02}. In the [27] the effect of hydrogen on the mechanical behavior of Cr−Mo-ferritic steel (2.5% Cr, 1% Mo) with different heat treatment was studied. The value of σ_{02} varied in the range from 430 to 761 MPa. The main mechanism of fracture of low-strength steel (430 MPa), even at the minimum tensile rate in the presence of hydrogen, was plastic, i.e., was due to the appearance, growth and coalescence of micropores. Small pores were observed in the central region of the fracture surface, the formation of which is associated with the mechanism of localized plasticity (HELP). For samples with the maximum strength of 761 MPa at a minimum loading rate, in addition to the above mechanisms, the development of fracture along the grain boundaries (IG) was observed.

Let us discuss the mechanism of fracture of pipe steels. In paper [32] the fracture surface of samples of ferritic steel with strength $\sigma_{02} < 550$ MPa, preliminarily charged with hydrogen, was studied. It is shown that under the surface of quasi-cleavage fracture sites at a distance of $< 2\,\mu$m from the surface, there is an extremely high density of dislocations, which extends through the entire grain. Along with the high density of dislocations, a developed subgrain structure with the grain size of 150−300 nm (the initial size of subgrains in steel not charged with hydrogen was $1-3\,\mu$m) was also found. This indicates that hydrogen activates many slip systems over a wide area, as expected in the HELP mechanism. It was also found that the fracture surface is covered with nanosized pores 5−20 nm in size and $1-5\,\mu$m deep. Note that nanopores occurred earlier than the moment of fracture due to the accumulation of vacancies during intense plastic deformation and the formation of hydrogen-vacancy agglomerations [6]. The junction of hydrogen-vacancy clusters leads to the formation of nanopores. Such nanopores are observed in the form of pits on the mating surfaces of quasi-brittle fracture regions. Based on the results of this work, a new HE mechanism (VM) based on hydrogen-induced localized plastic deformation was proposed; formation of nanopores by junction of hydrogen-vacancy clusters; their coalescence leading to the formation of micropores and subsequent quasi-brittle fracture. Thus, the proposed mechanism combines all three failure models HELP, HEDE and VM to explain HE in ferritic steels.

The bond between hydrogen and vacancy clusters and their influence on HE were studied not only for low-strength ferritic steels, but also for high-strength martensitic steels. It was shown [33] that under the surface of quasi-cleavage fracture elements along the block boundaries there are numerous nanopores formed from vacancy-hydrogen clusters that initiate intragranular fracture.

Note that the proposed hydrogen-vacancy mechanism for the micropores formation does not state calls into question the previously identified mechanisms HELP and HEDE, but only clarifies the mechanism of their action.

The above data show a noticeable difference in the corrosion behavior of low-strength ferritic steels from

that of high-strength steels. The main difference is that during corrosion testing of low-strength ferritic steels, both anodic dissolution (AD) and cathodic hydrogen reduction processes are accelerated. In this regard, let us discuss the data on the effect of stress and plastic deformation on the electrochemical behavior of low-strength steel X70 ($\sigma_{02} = 490$ MPa) [34].

It is known that the potential for electrochemical corrosion is affected by an external load. According to [35], in the region of elastic deformation the change in the electrode potential caused by the load is defined as

$$\Delta\varphi = \frac{\Delta P \cdot V_m}{zF}, \tag{1}$$

where ΔP is overpressure, V_m is molar volume of the alloy, z is ion valence, F is Faraday's constant. In the region of plastic deformation, the relationship between potential displacement and plastic deformation is defined as follows [36]:

$$\Delta\varphi = \frac{TR}{zF} \ln\left(\frac{\vartheta\alpha}{N_0}\varepsilon_p + 1\right), \tag{2}$$

where ϑ is orientation-dependent factor, α is coefficient, N_0 is dislocation density before deformation, ε_p is plastic deformation, T is temperature, R is gas constant.

It follows from the experimental data [34] that both stress and plastic deformation reduce the potential of the electrode, which leads to the corrosion activity increasing of the steel. From [34] for steel X70 tested at a strain rate of $1 \cdot 10^{-4}\,\mathrm{s}^{-1}$ in a neutral solution, it follows that in the region of elastic deformation, the decrease in the potential corrosion is negligible and amounts to $1mV_{\mathrm{SCE}}$. In the region of plastic deformation $\varepsilon_p = 20\%$ the negative shift of the potential is 10 times larger and amounts to $11mV_{\mathrm{SCE}}$. (The change in the potential $\Delta\varphi$ occurred linearly with strain increasing). The acceleration of the cathodic reaction is associated with the area increasing of the cathodic regions. It is also noted in paper [34] that the dislocation density increasing during plastic deformation additionally creates a large number of active centers on the surface (slip steps and bends on the surface), accelerating electrochemical reactions. According to [37], the number of dislocations reaching the surface in one grain is related to plastic deformation and grain size

$$n = \frac{Ld}{r_0^2}\varepsilon_p, \tag{3}$$

where r_0 is atomic radius, L and d are initial grain size and depth.

Note that the acceleration of stress corrosion is affected by surface defects, such as cleavage steps, microcracks, and other defects generated during plastic deformation. The integral characteristic of these defects is the roughness (R_a) of the sample surface, the value of which is related to plastic deformation ε_p and grain size d_0 by a linear dependence [38]:

$$R_a = R_{a_0} + k \cdot d_0 \cdot \varepsilon_p, \tag{4}$$

where k is coefficient.

It follows from (4) that with ε_p increase, the roughness of the steel surface increases. According to [39], the growth of R_a during corrosion will accelerate anodic and especially cathodic reactions in low-strength ferritic steels.

Thus, it was established that during plastic deformation of steel in the corrosion solution, both anodic and cathodic processes are accelerated. This process will be especially noticeable in low-strength ferritic steels with yield stress of less than 550 MPa, since the grain size L is related to the σ_{02} value by the Hall–Petch equation: $\sigma_{02} \sim L^{-1/2}$.

It is also shown that HE-of loaded steels of various compositions in sodium chloride solution occur already at the stage of anodic dissolution, regardless of the value of the anodic and cathodic potentials [40] due to acidification of the solution in the area of localized corrosion (pitting bottom or in the emerging microcrack) to a pH value of 3.8 [41].

Finally, the data on the change in the duration of the anodic dissolution stage in the NACE solution (t_{AD}) (Fig. 2) support the conclusion that the steels sensitivity to HE increases with the σ_{02} value change. Thus, it can be assumed that the transition from the AD stage to the SCC stage occurs with the accumulation of hydrogen at the initial stage of the test up to a certain critical value. In this case, the t_{AD} value decreasing observed in Fig. 2 indicates the hydrogen accumulation rate increasing when testing steels with the yield stress different from $\sigma_{02} = 550$ MPa, at which the rate of hydrogen accumulation is minimal.

The considered data show that plastic deformation in low-strength pipe steels increases the steel susceptibility to stress corrosion cracking by increasing the rate of anodic dissolution and increasing the hydrogen content in the steel. Increasing of HE degree is facilitated by the exit of dislocations on the surface, which enhances local corrosion and pitting. In turn, pittings are sites of crack initiation due to stress concentration, the magnitude of which, as shown by our estimates for low-alloy steels with strength σ_{02} below 550 MPa in NACE solution, is 4.1. Plastic deformation accelerates the restoration of hydrogen ions due to the fresh surface formation during plastic deformation. The dislocation density increasing leads to increasing of the number of reversible traps for hydrogen. Hydrogen penetrating into the steel together with dislocations, if a neck is created, can be attracted to the region of triaxial stresses ahead of the crack tip and contribute to its propagation.

Based on the data reviewed, the following conclusions can be drawn.

1. The bell-shaped nature of the dependence of the σ_{CR} value of the transition from the AD stage to the SCC stage is due to the activation of the cathodic process of hydrogen

reduction with increasing or decreasing of the yield stress from the value of $\sigma_{02} = 550$ MPa.

2. The yield stress value significantly affects the corrosion behavior of ferritic and martensitic steels in the NACE solution: the HE mechanism, the stress σ_{CR} and the transition time t_{AD} from active corrosion to the stage of stress corrosion cracking, as well as the value of threshold stress σ_{th}.

Conflict of interest

The authors declare that they have no conflict of interest.

References

[1] A.I. Petrov, M.V. Razuvaeva. Tech. Phys., **65** (12), 2035 (2020). DOI: 10.1134/S106378422012021X

[2] A.R. Troiano. Trans. Am. Soc. Met., **52**, 54 (1960). DOI: 10.1007/s13632-016-0319-4

[3] W.W. Gerberich, R.A. Oriani, M.-J. Lji, X. Chen, T. Foecke. Philosophical Magazine A, **63** (2), 363 (1991). DOI: 10.1080/01418619108204854

[4] R.A. Oriani. Corrosion, **43** (7), 390 (1987). DOI: 10.5006/1.3583875

[5] H.K. Birnbaum, P. Sofronis. Mater. Sci. Engineer. A, **176** (1−2), 191 (1994). DOI: 10.1016/0921-5093(94)90975-X

[6] M. Nagumo. ISIJ International, **41** (6), 590 (2001). DOI: 10.2355/isijinternational.41.590

[7] L. Jemblie, V. Olden, O.M. Akselsen. Intern. J. Hydrogen Energy, **42**, 11980 (2017). DOI: 10.1016/j.ijhydene.2017.02.211

[8] R.L.S. Thomas, D. Li, R.P. Gangloff, J.R. Scully. Metallurgical and Mater. Transactions A, **33A**, 1991 (2002). DOI: https://link.springer.com/article/10.1007/s11661-002-0032-6

[9] M. Dadfarnia, P. Sofronis, T. Neeraj. Intern. J. Hydrogen Energy, **36**, 10141 (2011). DOI: 10.1016/j.ijhydene.2011.05.027

[10] H.K.D.H. Bhadeshia. ISIJ International, **56** (1), 24 (2016). DOI: 10.2355/isijinternational.ISIJINT-2015-430

[11] A. Nagao, M. Dadfarnia, B.P. Somerday, P. Sofronis, R.O. Ritchie. J. Mechan. Phys. Solids, **112**, 403 (2018). DOI: 10.1016/j.jmps.2017.12.016

[12] T. Doshida, K. Takai. Acta Mater., **79**, 93 (2014). DOI: http://dx.doi.org/10.1016/j.actamat.2014.07.008

[13] T. Depover, E. Wallaert, K. Verbeken. Mater. Sci. Engineer. A, **664**, 195 (2016). DOI: http://dx.doi.org/10.1016/j.msea.2016.03.107

[14] C.D. Kim, A.W. Loginow. Corrosion, **24** (10), 313 (1968). DOI: 10.5006/0010-9312-24.10.313

[15] T. Depover, K. Verbcfecn. Intern. J. Hydrogen Energy, **43**, 3050 (2018). DOI: 10.1016/j.ijhydene.2017.12.109

[16] Q. Liu, Q. Zhou, J. Venezuela, M. Zhang, A. Atrens. Corrosion Sci., **125**, 114 (2017). DOI: http://dx.doi.org/10.1016/j.corsci.2017.06.012

[17] M. Dadfarnia, M.L. Martin, A. Nagao, P. Sofronis, l.M. Robertson. J. Mech. Phys. Solids, **78**, 511 (2015). DOI: http://dx.doi.org/10.1016/j.jmps.2015.03.002

[18] H.K. Birnbaum, P. Sofronis. Mater. Sci. Engineer. A, **176** (1−2), 191 (1994). DOI: 10.1016/0921-5093(94)90975-X

[19] P. Novak, R. Yuan, B.P. Somerday, P. Sofronis, R.O. Ritchie. J. Mechan. Phys. Solids, **58**, 206 (2010). DOI: 10.1016/j.jmps.2009.10.005

[20] M.L. Martin, M. Dadfarnia, A. Nagao, S. Wang, P. Sofronis. Acta Mater., **165**, 734 (2019). DOI: 10.1016/j.actamat.2018.12.014

[21] F.G. Wei, K. Tsuzaki. *Hydrogen Trapping Phenomena in Martensitic Steels, in book Gaseous HE of Materials in Energy Technologies*, ed. by R.P. Gangloff, B.P. Somerday. (Woodhead Publishing Limited, 2012), v. 2, p. 493–525. DOI: 10.1533/9780857093899.3.493

[22] D. Guedes, L. Cupertino Malheiros, A. Oudriss, S. Cohendoz, J. Bouhattate, J.F. Thebault, M. Piette, X. Feaugas. Acta Mater., **186**, 133 (2020). DOI: 10.1016/j.actamat.2019.12.045

[23] A. Nagao, C.D. Smith, M. Dadfarnia, P. Sofronis, I.M. Robertson. Acta Mater., **60** (13−14), 5182 (2012). DOI: http://dx.doi.org/10.1016/j.actamat.2012.06.040

[24] I.M. Robertson, P. Sofronis, A. Nagao, M.L. Martin, S. Wang, D.W. Gross, K.E. Nygren. Metall. Mater. Trans., **46A**, 2323 (2015). DOI: https://link.springer.com/article/10.1007/s11661-015-2836-1

[25] A. Oudriss, A. Fleurentin, G. Courlit, E. Conforto, C. Berziou, C. Rébéré, S. Cohendoz, J.M. Sobrino, J. Creus, X. Feaugas. Mater. Sci. Engineer.: A, **598**, 420 (2014). DOI: 10.1016/j.msea.2014.01.039

[26] N. Nanninga, J. Grochowsi, L. Heldt, K. Rundman. Corrosion Sci., **52**, 1237 (2010). DOI: 10.1016/j.corsci.2009.12.020

[27] L.B. Peral, A. Zafra, I. Ternandez-Pariente, C. Rodriguez, J. Belzunce. Intern. J. Hydrogen Energy, **45**, 22054 (2020). DOI: 10.1016/j.ijhydene.2020.05.228

[28] L. Wang, J. Xin, L. Cheng, K. Zhao, B. Sun, J. Li, X. Wangh, Z. Cui. Corrosion Sci., **147**, 108 (2019). DOI: 10.1016/j.corsci.2018.11.007

[29] Z.Y. Liu, X.G. Li, C.W. Du, L. Lu, Y.R. Zhang, Y.F. Cheng. Corrosion Sci., **51**, 895 (2009). DOI: 10.1016/j.corsci.2009.01.007

[30] L. Zhiyong, C. Zhongyu, L. Xiaogang, D. Cuiwei, X. Yunying. Electrochem. Commun., **48**, 127 (2014). DOI: 10.1016/j.elecom.2014.08.016

[31] A. Fragiel, S. Serna, J. Malo-Tamayo, P. Silva, B. Campillo, E. Martinez-Martinez, L. Cota, M.H. Staia, E.S. Puchi-Cabrera, R. Perez. Engineer. Failure Analysis, **105**, 1055 (2019). DOI: 10.1016/j.engfailanal.2019.06.028

[32] T. Neeraj, R. Srinivasan, Ju Li. Acta Mater., **60**, 5160 (2012). DOI: http://dx.doi.org/10.1016/j/actamat.2012.06.014

[33] M. Nagumo, K. Takai. Acta Mater., **165**, 722 (2019). DOI: 10.1016/actamat.2018.12.013

[34] Z. Cui, Z. Liu, L. Wang, X. Li, C. Du, X. Wang. Mater. Sci. Engineer. A, **677**, 259 (2016). DOI: 10.1016/j.msea.2016.09.033

[35] E.M. Gutman. *Mechanochemistry of Materials* (Cambridge Int Science Publishing, Cambridge, UK, 1998, 211 p.)

[36] L.Y. Xu, Y.F. Cheng. Corros. Sci., **64**, 145 (2012). DOI: 10.1016/j.corsci.2012.07.012

[37] Z.Y. Liu, X.G. Li, C.W. Du, Y.F. Cheng. Corrosion Sci., **51**, 2863 (2009). DOI: 10.1016/j.corsci.2009.08.019

[38] J. Dai, F. Chiang. J. Eng. Mater. Technol., **114**, 432 (1992). DOI: 10.1115/1.2904196

[39] H. Krawiec, V. Vignal, E. Schwarzenboeck, J. Banas. Electrochim. Acta, **104**, 400 (2013). DOI: 10.1016/j.electacta.2012.12.029
[40] B.E. Wilde. Corrosion, **27** (8), 326 (1971). DOI: 10.5006/0010-9312-27.8.326
[41] *Corrosion*, ed. by L.L. Shreir (Newnes-Butterworths, London, Boston) 632 p.